Ceramics International 45 (2019) 11756–11764

Contents lists available at ScienceDirect

Ceramics International

journal homepage: www.elsevier.com/locate/ceramint

In-situ pyrolyzed polymethylsilsesquioxane multi-walled carbon nanotubes derived ceramic nanocomposites for electromagnetic wave absorption

Lixin Chen[a], Jia Zhao[a], Lei Wang[a], Fei Peng[a], Hu Liu[c,d], Jiaoxia Zhang[c,e], Junwei Gu[a,b,**], Zhanhu Guo[c,*]

[a] MOE Key Laboratory of Material Physics and Chemistry under Extraordinary Conditions, Shaanxi Key Laboratory of Macromolecular Science and Technology, Department of Applied Chemistry, School of Science, Northwestern Polytechnical University, Xi'an, Shaanxi, 710072, China
[b] Institute of Intelligence Material and Structure, Unmanned System Research Institute, Northwestern Polytechnical University, Xi'an, Shaanxi, 710072, China
[c] Integrated Composites Laboratory (ICL), Department of Chemical & Biomolecular Engineering, University of Tennessee, Knoxville, TN, 37996, USA
[d] Key Laboratory of Materials Processing and Mold (Zhengzhou University), Ministry of Education, National Engineering Research Center for Advanced Polymer Processing Technology, Zhengzhou University, Zhengzhou, 450002, China
[e] School of Material Science and Engineering, Jiangsu University of Science and Technology, Zhenjiang, Jiangsu, 212003, China

ARTICLE INFO

Keywords:
Ceramic composites
Polymer-derived ceramics
Microwave-absorbing property
Multi-walled carbon nanotubes
SiC nanocrystals

ABSTRACT

Iron acetylacetonate ($Fe(acac)_3$) modified polymethylsilsesquioxane (PMS), simplified as PMS(Fe), was firstly obtained from PMS and $Fe(acac)_3$ *via* the condensation reaction. Multi-walled carbon nanotubes (MWCNTs) were then introduced to fabricate the corresponding MWCNTs/SiC nanocrystals/amorphous SiOC ceramic composites *via* pyrolyzed process. Owing to the catalytic effect of iron and heterogeneous nucleation promoted by MWCNTs, SiC nanocrystals were separated from SiOC amorphous ceramic matrix under 1400 °C. When the mass fraction of MWCNTs was 9 wt%, the obtained MWCNTs/SiC nanocrystals/amorphous SiOC ceramic composite (C9) demonstrated high microwave-absorbing properties. The minimum reflection loss (RL_{min}) and effective absorption bandwidth (EBA) of the obtained C9 at X-band (8.2–12.4) reached −61.8 dB and 2.6 GHz (a thickness of 2.19 mm), respectively. Compared with other polymer-derived ceramics (PDCs), the RL_{min} was higher and the required thickness was thinner. This excellent microwave-absorbing property was due to the interfacial polarization relaxation generated between nanocrystals (MWCNTs & SiC) and amorphous SiOC, and the formed complete conductive networks inside the ceramic composites.

1. Introduction

With the rapid development of science & technology, the electromagnetic technology has been utilized in many fields, such as data transmission, satellite launch and radar technology, *etc.* In order to eliminate the influence of electromagnetic interference (EMI) on the electronics in our normal work and human life, and to satisfy the development of stealth technology, high performance microwave-absorbing materials, presenting both low reflection loss (RL) and broad effective absorbing bandwidth (EBA), are urgently required [1–8]. The weather radar, Doppler, telephone microwave relay systems and military applications all refer to the X-band (8.2–12.4 GHz), therefore, the design and preparation of high performance microwave-absorbing materials at X-band have attracted much attention [9,10]. To obtain good impedance matching and strong microwave-absorbing capability, microwave-absorbing materials should contain the electrically lossy phase and electrically insulating phase. To the best our knowledge, polymer-derived ceramics (PDCs) are promising candidates, due to their semiconductor (SiC) and electrically conductive phase (graphite carbon) scattered in amorphous matrix (amorphous SiC, SiOC, SiCN or SiBCN) [11,12].

In the past recent years, PDCs technology has received considerable concerns [13–15]. PDCs route mainly includes three steps: crosslinked process of polymers, conversion from crosslinked polymers to amorphous ceramics, and the formation of crystalline ceramics by high temperature annealing treatment. In contrast with traditional processes, PDCs route presents the advantages of low processing temperature and controlled ceramic shape [16–19]. Additionally, owing to high strength & temperature resistance, excellent corrosion resistance and good oxidation resistance of PDCs (PDC-SiC, PDC-SiCN, PDC-SiOC),

* Corresponding author.
** Corresponding author. MOE Key Laboratory of Material Physics and Chemistry under Extraordinary Conditions, Shaanxi Key Laboratory of Macromolecular Science and Technology, Department of Applied Chemistry, School of Science, Northwestern Polytechnical University, Xi'an, Shaanxi, 710072, China.
E-mail addresses: gjw@nwpu.edu.cn, nwpugjw@163.com (J. Gu), nanomaterials2000@gmail.com, zguo10@utk.edu (Z. Guo).

https://doi.org/10.1016/j.ceramint.2019.03.052
Received 23 February 2019; Received in revised form 2 March 2019; Accepted 8 March 2019
Available online 12 March 2019
0272-8842/

PDCs are endowed with a broad application prospect (ceramic fiber, ceramic matrix composite, ceramic film, *etc*) [13]. However, because of high chemical and thermal stability of PDCs derived from pure polymers, few conductive and semi-conductive materials are separated from amorphous matrix, and the corresponding microwave-absorbing properties are very poor, even processed at a temperature up to 1400 °C. To our knowledge, incorporating fillers into ceramic precursors can effectively improve their microwave-absorbing properties. The above fillers can be divided into transition metals (iron, cobalt and nickel, *etc*) and electrically conductive nano fillers (SiC, TiC and CNTs, *etc*) [20–28].

For example, Luo et al. [21] prepared microwave-absorbing PDCs through pyrolysis of cobalt coordinated poly(dimethylsilylene)diacetylenes, the minimum RL and corresponding EBA could reach −42.78 dB and 2.37 GHz, respectively (a thickness of 2.65 mm). Duan et al. [22] fabricated SiC nanowires reinforced SiOC ceramics by pyrolysis of polysiloxane containing ferrocene. With the increase of SiC nanowires content, the real permittivity and the imaginary permittivity could reach 10.12 and 12.17, respectively, and the minimum RL could reach −20.01 dB at a thickness of 3.3 mm. Zhang et al. [23] fabricated polymer-derived siliconboron carbonitride ceramics (PDC-SiBCN) containing multi-walled carbon nanotubes (MWCNTs). When the annealing temperature was 1350 °C, the minimum RL and EBA reached −13 dB and 1.5 GHz, respectively at a thickness of 2.8 mm. Ye et al. [24] fabricated PDC-SiBCN doped nano SiC having enhanced permittivity and low RL. The SiC/SiBCN ceramics were composed of SiC nanoparticles and amorphous SiBCN, and the minimum RL could reach −19.7 dB at a thickness of 7 mm. To summarize, the current researches mainly focus on the introduction of single fillers. It is obvious that the introduction of transition metals will increase the density of materials and the introduction of electrically conductive nano fillers will need the consideration about dispersibility of nanomaterials. However, strong microwave-absorbing properties require the introduction of a certain amount of single fillers. Based on above problems, combining transition metals and electrically conductive nano fillers would be a facile and efficient method to achieve excellent microwave-absorbing properties under the premise of less consumption for each filler.

In the present work, iron acetylacetonate ($Fe(acac)_3$) modified polymethylsilsesquioxane (PMS), simplified as PMS(Fe), was firstly obtained from PMS and $Fe(acac)_3$ *via* the condensation reaction and the MWCNTs/SiC nanocrystals/amorphous SiOC ceramic microwave-absorbing materials were then fabricated *via* pyrolysis of PMS(Fe) containing MWCNTs. Herein, the microstructures, phase compositions, electromagnetic properties and microwave-absorbing properties of the obtained MWCNTs/SiC nanocrystals/amorphous SiOC ceramic composites were investigated and the enhanced microwave absorption was analyzed in detail.

2. Experimental

2.1. Materials

Polymethylsilsesquioxane (PMS) was supplied by Shanghai Soft Chemical Co., Ltd. Iron acetylacetonate ($Fe(acac)_3$) was purchased from Strem Chemicals Co., Ltd. Multi-walled carbon nanotubes (MWCNTs, OD:8–15 nm, Length: 10–50 μm) were provided by Chengdu Organic Chemicals Co., Ltd.

2.2. Fabrication of MWCNTs/SiC nanocrystals/amorphous SiOC ceramic composites

Firstly, PMS and $Fe(acac)_3$ were used to fabricate PMS(Fe) (mass ratio of Fe was 3 wt%) *via* the condensation reaction, schematically presented in Fig. 1. Herein, PMS and $Fe(acac)_3$ were mixed using alcohol as solvent and stirred for 4 h. Then, the solvent was naturally evaporated under stirring followed by drying in a vacuum oven. Afterward, MWCNTs were dispersed in alcohol under ultrasonication, and PMS(Fe) was then added into the above dispersion liquid and maintained stirring for another 12 h. After the removal of alcohol, the PMS(Fe) containing MWCNTs was crosslinked at argon atmosphere at 400 °C for 3 h. The crosslinked products were ball milled for 4 h and then were pressed into bulk ceramics under 20 MPa. The bulk ceramic was pyrolyzed at 1400 °C for another 2 h, finally to obtain the MWCNTs/SiC nanocrystals/amorphous SiOC ceramic composites. The preparation process was shown in Fig. 2.

To investigate the effects of MWCNTs content on the microwave-absorbing properties of the obtained ceramic composites, a series of MWCNTs/SiC nanocrystals/amorphous SiOC ceramic composites with different MWCNTs content were fabricated (as shown in Table 1). The MWCNTs content was 0%, 3%, 5%, 7% and 9%, the corresponding ceramic composite was labeled as C0, C3, C5, C7 and C9, respectively. For comparison, the ceramic derived from pure PMS was abbreviated as Cp.

2.3. Characterization

Fourier transform infrared (FTIR) spectra of the samples were obtained on a Bruker Tensor 27 equipment (Bruker Co., Germany) with thin films on KBr [29]. Thermogravimetric analysis (TGA) of the samples were performed by a thermal gravimetric analyzer (SDT Q600, TA Corp., America) at 10 °C/min (argon atmosphere, 25–1400 °C or air condition, 50–900 °C). X-ray diffraction (XRD) analyses of the samples were carried out on an X-ray diffractometer (Bruker AXS, Germany) with Cu Ka radiation (λ = 0.154 nm). Raman spectra measurements of the samples were conducted by a Raman spectrometer (Renishaw 2000) with λ = 514.5 nm. Transmission electron microscope (TEM) morphologies of the samples were implemented by a field emission high resolution transmission electron microscopy (FEI Talos F200X) at 200 kV. The samples for analysis were dispersed in alcohol and deposited on a holey Cu/carbon grid.

The complex permittivity ($\varepsilon_r = \varepsilon' - j\varepsilon''$) and complex permeability ($\mu_r = \mu' - j\mu''$) for the samples (dimension of 22.86 mm × 10.16 mm × 2.2 mm) were measured using a vector network analyzer (VNA, Agilent Technologies E8362B) at X-band (8.2–12.4 GHz) by wave-guide method. Direct current (DC) conductivities were tested using four point probe method.

3. Results and discussion

3.1. Characterization of $Fe(acac)_3$ modified PMS

Fig. 3**(a)** shows the FTIR curves of PMS and $Fe(acac)_3$ modified PMS (PMS(Fe)). For pure PMS, the vibration absorption peak at 768/1274 cm^{-1}, 1121 cm^{-1} and 1032 cm^{-1} is assigned to the Si—CH_3, Si—O—Si and Si—O—C, respectively [30–32]. Owing to the acetylacetonate ligands of $Fe(acac)_3$, some new vibration absorption bands at 1572 cm^{-1} (C═O), 1526 cm^{-1} (C═C), and 667 cm^{-1} (Fe—O) are observed in PMS(Fe) [33,34]. In addition, the vibration absorption band at 930 cm^{-1} for Si—O—Fe also reveals the condensation reaction between $Fe(acac)_3$ and Si—OH of PMS [35].

Fig. 3**(b)** shows the XRD patterns of Cp derived from pure PMS and C0 derived from PMS(Fe). The observed broad peak at 2θ = 20–30° for the Cp indicates that the ceramics derived from pure PMS are SiOC amorphous phase. For the C0 derived from PMS(Fe), the observed diffraction peaks at 21.8°, 35.6°, 41.3°, 45.3°, 59.9° and 71.8° correspond to the 101 lattice plane of SiO_2, 111 lattice plane of β-SiC, 200 lattice plane of β-SiC, 211 lattice plane of Fe_5Si_3, 220 lattice plane of β-SiC, and 311 lattice plane of β-SiC, respectively [20,36]. The formation of β-SiC is due to the carbothermal reduction ($SiO_2(s) + 3C(s) \rightarrow SiC(s) + 2CO(g)$) [37–39]. And the existence of iron not only improves the reactive activity of SiO_2, but also forms the Fe—Si melt, finally promotes the formation of β-SiC [40].

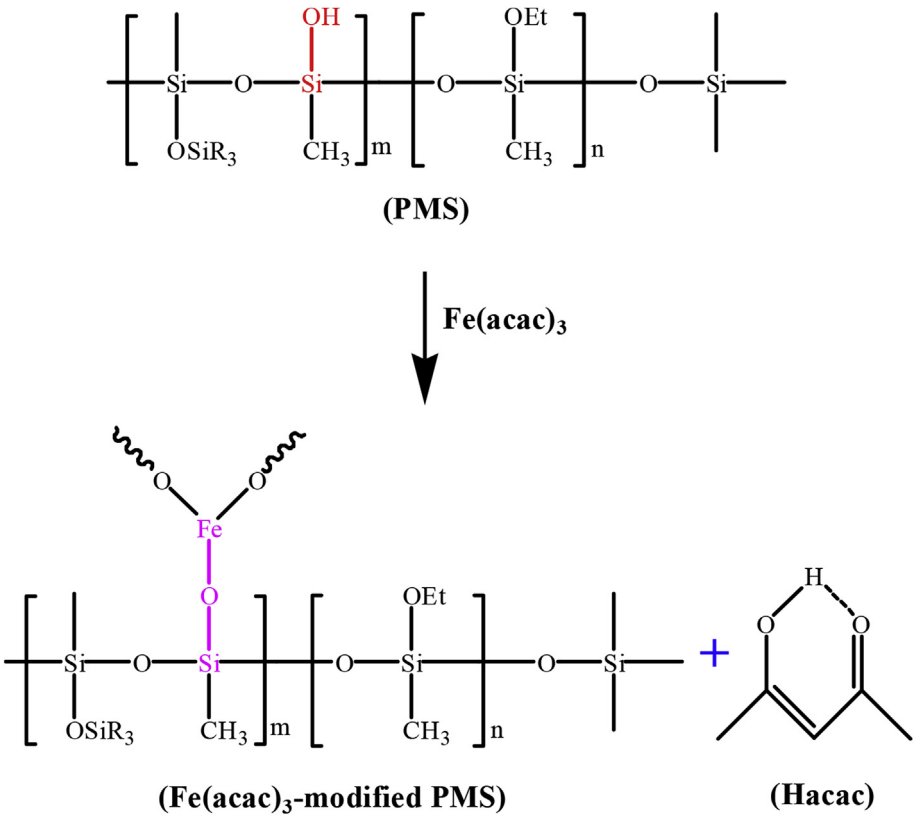

Fig. 1. Schematic diagram of synthesis process for $Fe(acac)_3$-modified PMS.

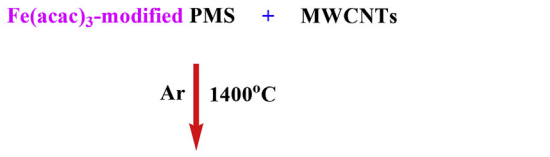

Fig. 2. Schematic diagram of preparation process for MWCNTs/SiC nanocrystals/amorphous SiOC ceramic composites.

Table 1
Experiment design of ceramics derived from polymeric precursors.

Ceramics	Precursors	Temperature (°C)
Cp	PMS	1400
C0	PMS(Fe) + 0%MWCNTs	1400
C3	PMS(Fe) + 3%MWCNTs	1400
C5	PMS(Fe) + 5%MWCNTs	1400
C7	PMS(Fe) + 7%MWCNTs	1400
C9	PMS(Fe) + 9%MWCNTs	1400

3.2. Pyrolysis processes of $Fe(acac)_3$ modified PMS containing MWCNTs in Ar atmosphere

The pyrolysis processes of $Fe(acac)_3$ modified PMS (PMS(Fe)) containing MWCNTs are investigated. Fig. 4 shows the TGA curves of PMS (Fe) containing MWCNTs in Ar atmosphere. The corresponding pyrolysis processes are divided into three steps. The weight loss of the first stage (25–600 °C) is near 2%, mainly ascribed to the released non-crosslinked small molecules. At the second stage (600–800 °C), the weight loss corresponds to the breakage and rearrangement of molecular chains. At the third stage (800–1400 °C), the corresponding weight loss reaches 17%, attributed to the carbothermal reduction [22,36]. With increasing the addition of MWCNTs, the yields of the MWCNTs/SiC nanocrystals/amorphous SiOC ceramic composites at 1400 °C are decreased gradually, mainly attributed to the accelerated heterogeneous nucleation of SiC nanocrystals by introducing MWCNTs [23,41]. Specifically, a large number of heterogeneous interfaces between MWCNTs and SiOC amorphous phase would be in favor of carbothermal reduction. Even so, the yield of the above ceramic composites with 9 wt% MWCNTs is as high as 72.9%. To exclude the influence of mass loss for MWCNTs during pyrolysis process, TGA curve of MWCNTs in Ar atmosphere is also supplied in Fig. 4. It can be seen that there is no obvious weight loss before 800 °C and the weight loss (2.42%) between 800 and 1400 °C is smaller than that (7.6%) of PMS (Fe). This result further indicates the accelerated heterogeneous nucleation of SiC nanocrystals by introducing MWCNTs.

3.3. Microstructures and thermal stabilities of the MWCNTs/SiC nanocrystals/amorphous SiOC ceramic composites

Fig. 5**(a)** shows the XRD patterns of MWCNTs/SiC nanocrystals/amorphous SiOC ceramic composites. All the samples exhibit diffraction peaks of SiO_2 ($2\theta = 21.6°$), β-SiC ($2\theta = 35.5°$, 41.4°, 59.9°, 71.7°) and Fe_5Si_3 ($2\theta = 45.3°$). Herein, the wide peak between 20° and 30° represents the SiOC amorphous phase. With the introduction of MWCNTs, an additional diffraction peak at $2\theta = 26.4°$ appears, and the corresponding intensity is also increased gradually with increasing the addition of MWCNTs. In addition, the corresponding diffraction peak intensity for SiO_2 presents a decreasing trend and all diffraction peaks for SiC present an increasing trend, mainly ascribed to the improvement effect of MWCNTs on the heterogeneous nucleation of SiC.

Fig. 5**(b)** shows the Raman spectra of MWCNTs/SiC nanocrystals/amorphous SiOC ceramic composites. Both D band near 1350 cm^{-1} representing the defects in the lattice of carbon atoms and the G band near 1590 cm^{-1} representing in-plane stretching vibration of sp^2 carbon atoms are observed. The corresponding I_D/I_G ratio values are

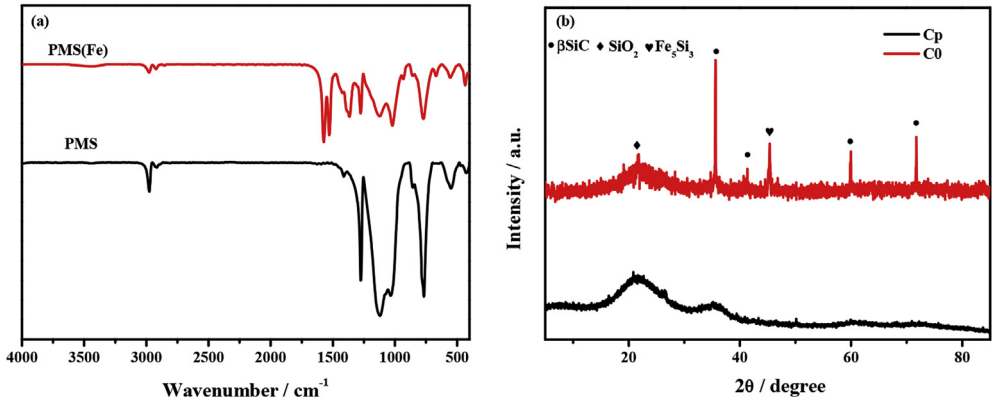

Fig. 3. FTIR curves (a) of PMS and Fe(acac)$_3$ modified PMS; XRD patterns (b) of amorphous SiOC ceramics (sample Cp) derived from pure PMS and SiC nanocrystals/amorphous SiOC ceramic composite (sample C0) derived from Fe(acac)$_3$ modified PMS.

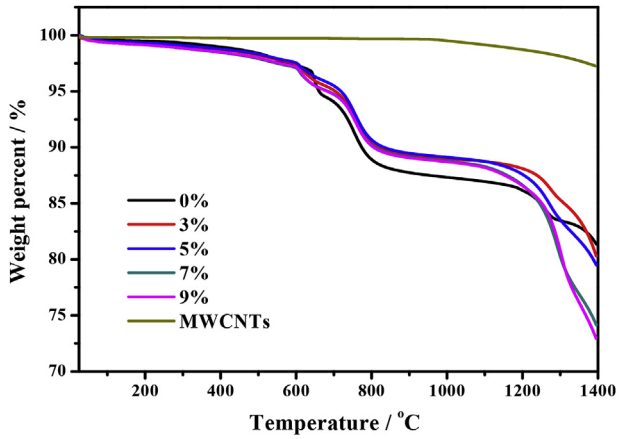

Fig. 4. TGA curves of the Fe(acac)$_3$ modified PMS containing MWCNTs and pristine MWCNTs in Ar atmosphere.

calculated and obtained by Gaussian-Lorentzian fitting [42–46]. In this work, I_D/I_G ratio value of MWCNTs and C0 is 0.31 and 2.21, respectively. With increasing the addition of MWCNTs, the corresponding I_D/I_G ratio values present a decreasing trend, indicating the increased MWCNTs content in the ceramic composites, consistent with the above XRD analyses.

The thermal stabilities of the MWCNTs/SiC nanocrystals/amorphous SiOC ceramic composites in air atmosphere are studied. Fig. 5**(c)** shows the TGA curves in air atmosphere of the MWCNTs/SiC nanocrystals/amorphous SiOC ceramic composites. No obvious weight loss for SiC nanocrystals/amorphous SiOC ceramic composites (C0) indicates that the obtained ceramic composites maintain high stability in air atmosphere even at 900 °C. After adding MWCNTs, MWCNTs/SiC nanocrystals/amorphous SiOC ceramic composites also have no obvious weight loss before 600 °C, and the weight loss (600–900 °C) corresponds to the oxidation of MWCNTs in the high temperature. The residual content at 900 °C for all MWCNTs/SiC nanocrystals/amorphous SiOC ceramic composites is over 90%, illustrating excellent thermal stabilities of the MWCNTs/SiC nanocrystals/amorphous SiOC ceramic composites in air atmosphere.

According to the above analyses, the schematic diagram of formation mechanism for MWCNTs/SiC nanocrystals/amorphous SiOC ceramic composite is shown in Fig. 6. Amorphous SiOC ceramic is derived from pure PMS. For Fe(acac)$_3$ modified PMS (PMS(Fe)), the SiC nanocrystals are separated from amorphous SiOC ceramics matrix owing to the catalytic effect of iron on the carbothermal reduction during pyrolysis process. After adding MWCNTs into Fe(acac)$_3$ modified PMS, a number of heterogeneous interfaces between MWCNTs and amorphous SiOC are formed in the corresponding ceramic composites. These heterogeneous interfaces can promote the heterogeneous nucleation of SiC and achieve further formation of SiC nanocrystals [23]. Therefore, more SiC nanocrystals and introduced MWCNTs are scattered in the amorphous SiOC ceramic matrix to form MWCNTs/SiC nanocrystals/amorphous SiOC ceramic composites.

3.4. Electromagnetic and microwave-absorbing properties of amorphous SiOC ceramics and MWCNTs/SiC nanocrystals/amorphous SiOC ceramic composites

The complex permittivity ($\varepsilon_r = \varepsilon' - j\varepsilon''$), complex permeability ($\mu_r = \mu' - j\mu''$), dielectric loss tangent ($\tan\delta\varepsilon = \varepsilon''/\varepsilon'$) and magnetic loss tangent ($\tan\delta\mu = \mu''/\mu'$) are the important parameters to characterize and predict the microwave-absorbing properties of the materials. Fig. 7 **s**hows the complex permeability of the amorphous SiOC ceramics derived from pure PMS and MWCNTs/SiC nanocrystals/amorphous SiOC ceramic composites. For all samples, the real permeability is close to 1. The imaginary permeability and magnetic loss tangent are close to 0, which indicates that magnetic losses of the amorphous SiOC ceramics and MWCNTs/SiC nanocrystals/amorphous SiOC ceramic composites are too small to be ignored. For amorphous SiOC ceramics derived from pure PMS, negative values appearing in the imaginary permeability and magnetic loss tangent are ascribed to no magnetic materials. For MWCNTs/SiC nanocrystals/amorphous SiOC ceramic composites, negative values appearing in the imaginary permeability and magnetic loss tangent are due to the fact that few iron is introduced (3%) [20,22]. In addition, the permeability of magnetic materials mainly was reflected in the low frequency band. However, X-band belongs to high frequency range [47].

Fig. 8(a) shows the DC conductivity of the amorphous SiOC ceramics derived from pure PMS and MWCNTs/SiC nanocrystals/amorphous SiOC ceramic composites. Owing to SiC nanocrystals separated from amorphous SiOC, the DC conductivity of C0 is slightly higher than Cp. And the DC conductivity shows an increasing tendency with increasing the addition of MWCNTs. The MWCNTs/SiC nanocrystals/amorphous SiOC ceramic composite (C9) possesses the maximum DC conductivity of 0.46 S/m. It is ascribed to the introduction of more MWCNTs and further formation of the SiC nanocrystals. The MWCNTs and SiC semiconductor can form the conductive networks, beneficial for the current flowing.

Fig. 8**(b)-(d)** shows the complex permittivity and loss tangent of the amorphous SiOC ceramics derived from pure PMS and MWCNTs/SiC nanocrystals/amorphous SiOC ceramic composites. The average value of dielectric loss tangent of amorphous SiOC ceramics (Cp) is 0.04. And for the SiC nanocrystals/amorphous SiOC ceramic composite (C0), the dielectric loss tangent increases to 0.11 owing to the formation of SiC nonacrystals in C0. The real permittivity, imaginary permittivity and

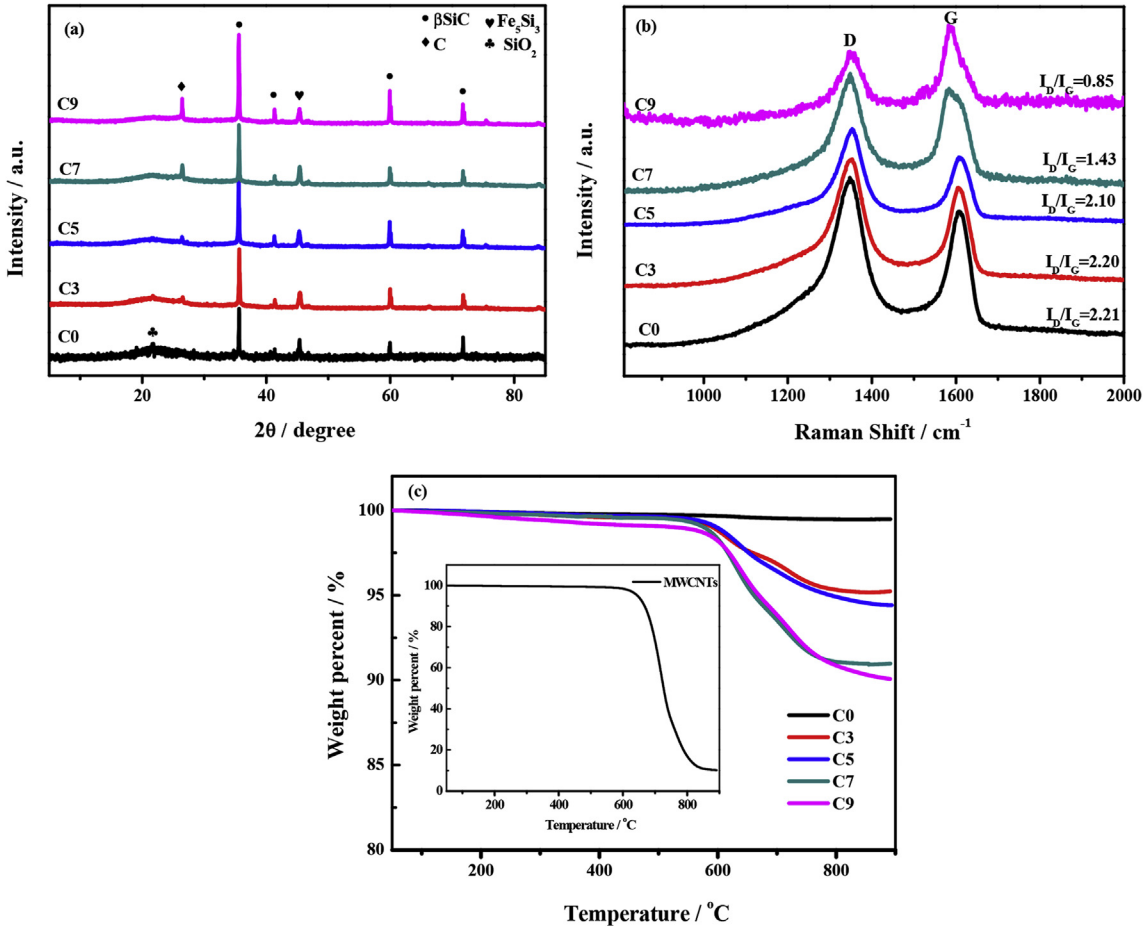

Fig. 5. XRD patterns (a), Raman spectra (b) and TGA curves in Air atmosphere (c) of the MWCNTs/SiC nanocrystals/amorphous SiOC ceramic composites (C0−C9).

dielectric loss tangent all show an increasing trend with the increasing addition of MWCNTs (C0−C9). The average value of ε' increases from 6.11 to 13.01, ε" increases from 0.68 to 4.33, and tanδ increases from 0.11 to 0.33. The improvement of permittivity is attributed to the increasing addition of MWCNTs and the further formation of SiC nanocrystals in the ceramic composites.

According to Maxwell-Wagner effect, the charges are accumulated at interfaces, and interfacial polarization relaxation is generated under external electromagnetic field and can improve the dielectric loss, helpful for the improvement of microwave-absorbing properties [48,49]. In this experiment, SiC nanocrystals/amorphous SiOC ceramic composite (C0) has a higher dielectric loss than amorphous SiOC ceramics (Cp) owing to the interfacial polarization caused by SiC nanocrystals in C0. For MWCNTs/SiC nanocrystals/amorphous SiOC ceramic composites (C3−C9), more SiC nanocrystals and introduced MWCNTs in ceramic composites can generate more interfacial polarization relaxation between nanocrystal phase and amorphous SiOC phase under external electromagnetic field, which can produce higher dielectric loss to absorb microwave. Additionally, the conductive network formed by SiC nanocrystals and MWCNTs in ceramic composites is also beneficial to the improvement of dielectric property.

Reflection loss (RL) can be calculated according to Equation (1&2):

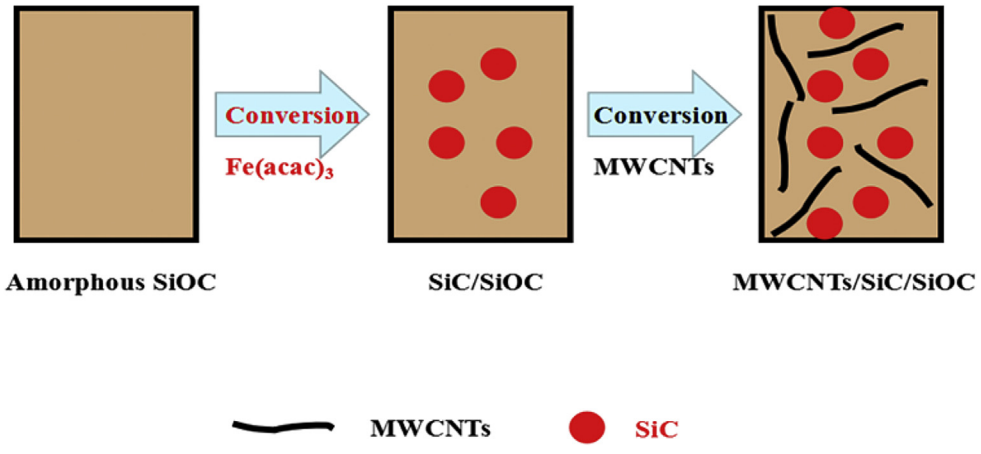

Fig. 6. Schematic diagram of generation mechanism for MWCNTs/SiC nanocrystals/amorphous SiOC ceramic composites.

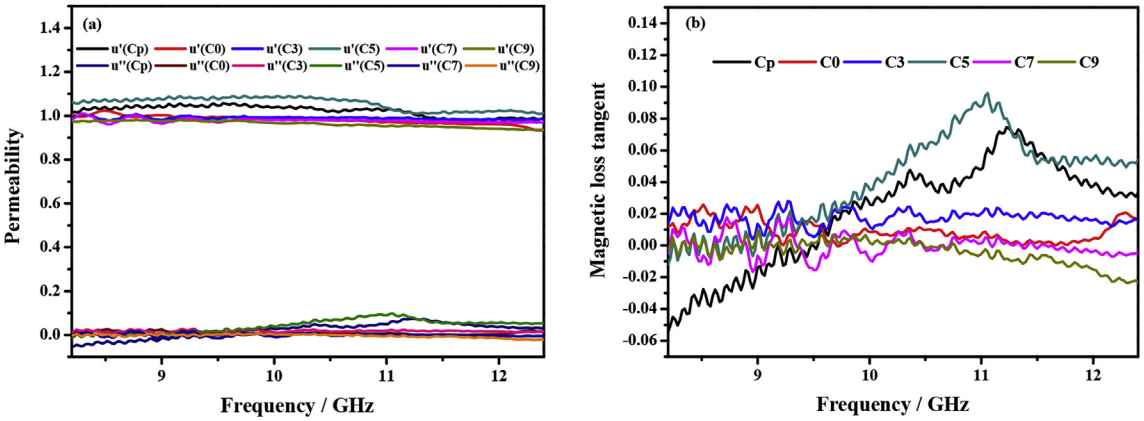

Fig. 7. Complex permeability (a) and magnetic loss tangent (b) of the pure amorphous SiOC ceramics (Cp) and MWCNTs/SiC nanocrystals/amorphous SiOC ceramic composites (C0−C9).

$$RL = 20\log_{10}|(Z_{in} - 1)/(Z_{in} + 1)| \quad (1)$$

$$Z_{in} = \sqrt{\mu_\gamma/\varepsilon_\gamma}\tanh\left(2\sqrt{\varepsilon_\gamma\mu_\gamma}fd\pi j/c\right) \quad (2)$$

where f, d and c represents microwave frequency, thickness and light velocity in vacuum, respectively. Z_{in} represents the normalized input impedance, ε_r and μ_r represent the complex permittivity and complex permeability, respectively [11,20].

Fig. 9**(a)** shows the RL values of the amorphous SiOC ceramics derived from pure PMS and MWCNTs/SiC nanocrystals/amorphous SiOC ceramic composites (a thickness of 2.2 mm). Cp is amorphous and its conductivity is very low according to above analyses, leading to the poor microwave-absorbing property. After the formation of SiC nanocrystals in C0, there is a certain improvement for microwave-absorbing property [12,20,22]. This phenomenon is ascribed to two aspects [23]: (i) The interfaces between SiC nanocrystals and amorphous SiOC can generate interface polarization, which can consume electromagnetic wave under external electromagnetic field. (ii) As shown in Fig. 8**(a)**, the formation of semiconductor SiC can increase the conductivity of the ceramic composites, which can also generate electric conductive loss to absorb electromagnetic wave. The microwave-absorbing properties of

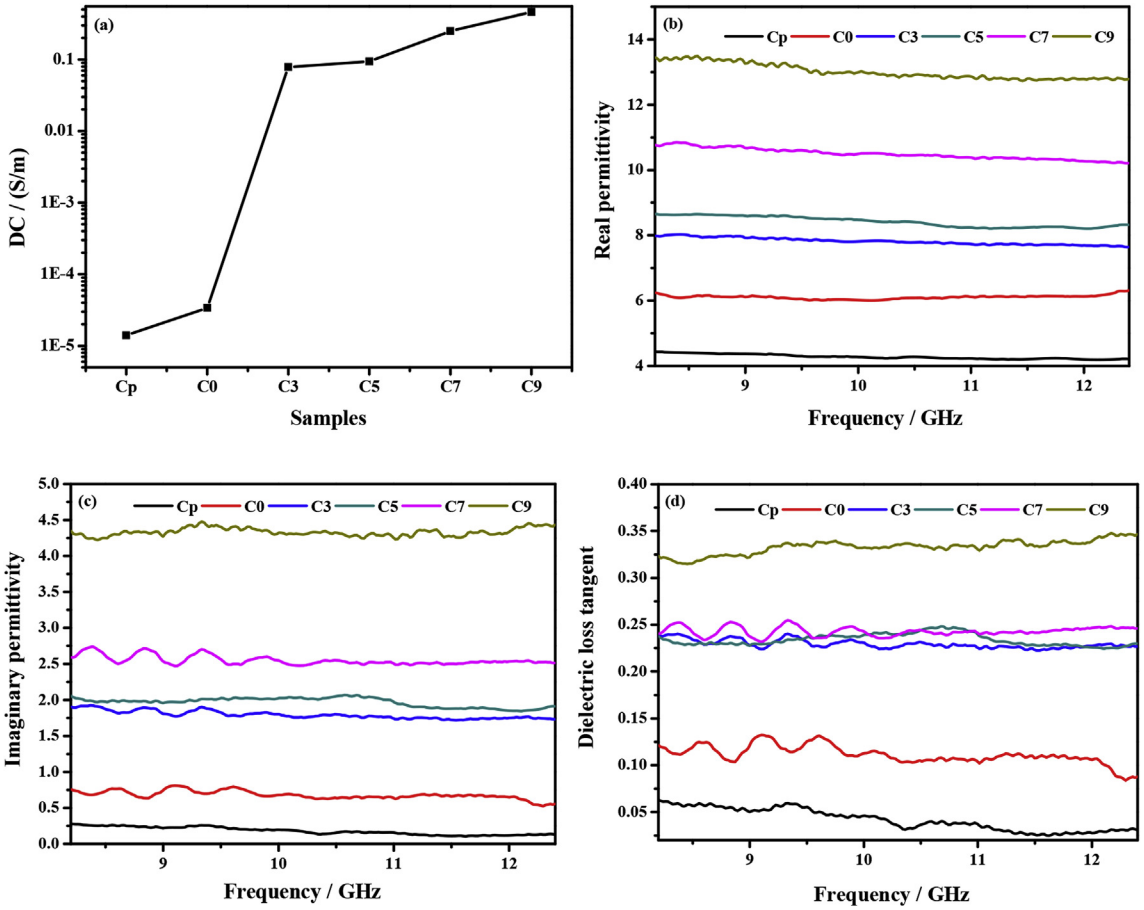

Fig. 8. DC conductivity (a), real permittivity (b), imaginary permittivity (c) and loss tangent (d) of the pure amorphous SiOC ceramics (Cp) and MWCNTs/SiC nanocrystals/amorphous SiOC ceramic composites (C0−C9).

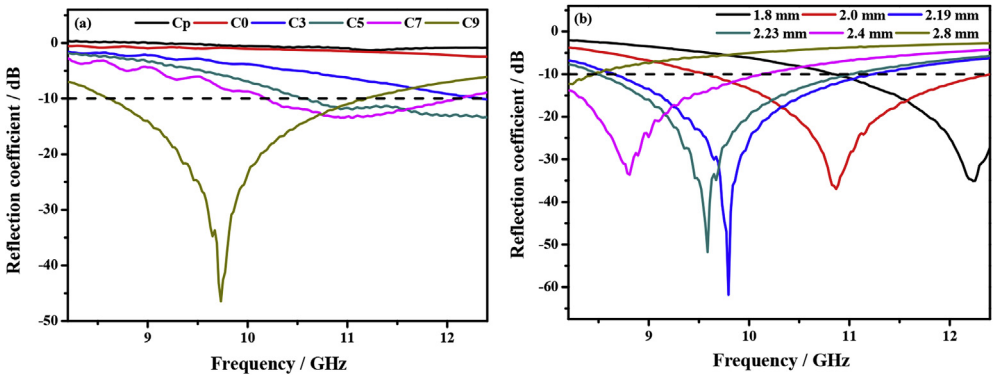

Fig. 9. RL values (a) of the pure amorphous SiOC ceramics (Cp) and MWCNTs/SiC nanocrystals/amorphous SiOC ceramic composites (C0−C9) (a thickness of 2.2 mm); RL values (b) of the MWCNTs/SiC nanocrystals/amorphous SiOC ceramic composite (C9) with different thickness.

the MWCNTs/SiC nanocrystals/amorphous SiOC ceramic composites are increased with increasing the addition of MWCNTs (C0−C9). C9 exhibits the optimal microwave-absorbing property, i.e., the corresponding minimum RL and EBA reach −46.45 dB and 2.56 GHz, respectively, mainly ascribed to the enhanced dielectric loss caused by further formation of SiC and introduction of MWCNTs. Moreover, the sample's thickness plays an important role in the microwave-absorbing properties. When the thickness of sample is at odd times of a quarter wavelength, the resonance of electromagnetic waves will occur on the surface of materials, to cause the absorption of electromagnetic waves [50]. Fig. 9**(b)** shows the RL of the MWCNTs/SiC nanocrystals/amorphous SiOC ceramic composite (C9) with different thicknesses. For a satisfied thickness (2.19 mm), the obtained ceramic composites exhibit the optimal microwave-absorbing property considering the minimum RL (−61.8 dB) and EBA (2.6 GHz).

Fig. 10 shows the corresponding TEM images of the MWCNTs/SiC nanocrystals/amorphous SiOC ceramic composite (C9). The MWCNTs and SiC nanocrystals are scattered uniformly inner C9. Thus, a large number of nanograin boundaries between MWCNTs/amorphous SiOC or SiC nanograins/amorphous SiOC are formed, and can generate interfacial polarization relaxation under external electromagnetic field. Additionally, the conductive network formed by SiC nanocrystals and MWCNTs in the C9 can also generate dielectric loss. Therefore, microwave can be absorbed and transformed into heat energy in the C9.

Based on the previous literature works, the relevant research data on microwave-absorbing properties of the ceramic composites are summarized in Table 2. The MWCNTs/SiC nanocrystals/amorphous SiOC ceramic composites produced in this work possess a very low RL (−61.8 dB) and broad EBA (2.6 GHz) at X-band. The RL_{min} (−61.8 dB) is better than that of most polymer-derived ceramics (PDCs). Most importantly, there are few papers to achieve strong absorption under the condition with the thickness being less than 2.5 mm for ceramic composites. Therefore, the obtained ceramic composites have promising potential in the field of electromagnetic interference (EMI) protection. It is attributed to the fact that MWCNTs and SiC nanocrystals in ceramic composites not only generate many interfacial polarization relaxation, but also form relatively complete conductive networks.

4. Conclusions

MWNTs/SiC nanocrystals/amorphous SiOC microwave-absorbing ceramic composites were successfully prepared using $Fe(acac)_3$ modified PMS containing MWCNTs as ceramic precursors by polymer-derived ceramics route. Owing to catalytic effect of iron and heterogeneous nucleation promoted by MWCNTs, the SiC nanocrystals were separated from SiOC amorphous ceramic matrix under 1400 °C. The increasing addition of MWCNTs was not only helpful for the formation of conductive networks, but also beneficial for the formation of more heterogeneous interfaces between nanocrystals and amorphous SiOC in the ceramic composites, which promoted the DC conductivities and dielectric properties of the ceramic composites. When the mass fraction of MWCNTs was 9 wt%, the obtained MWCNTs/SiC nanocrystals/amorphous SiOC ceramic composites (C9) exhibited a great microwave-absorbing behavior with the minimum reflection loss (RL) of −61.8 dB and effective absorption bandwidth (EBA) of 2.6 GHz (a thickness of

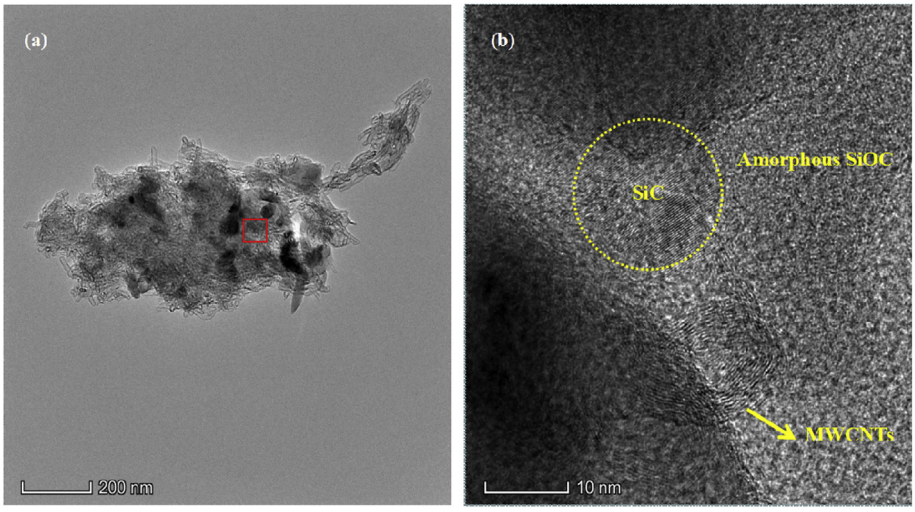

Fig. 10. TEM images of the MWCNTs/SiC nanocrystals/amorphous SiOC ceramic composite (C9).

Table 2
Microwave-absorbing properties of the ceramic composites.

Ceramic composites	ε'	ε''	RL_{min} (dB)	EAB (GHz)	Matching thickness (mm)	Ref
C/SiC/amorphous SiC	3.6–10.3	0.17–10	−9.9	0 (4.2)	2.75	[12]
C/SiC/TiC/amorphous SiC	~11.9	~4.5	/	/	/	[51]
MWCNTs/SiC/amorphous SiBCN	2.7–15.6	0.1–15.6	−32	3 (4.2)	2.5	[23]
C/SiC/amorphous SiCN	4.3–14.1	0.2–6.5	−53	3.02 (4.2)	3.35	[11]
C/SiC/amorphous SiOC	3.6–5.6	0.1–1.3	−10	0.06 (4.2)	4	[22]
C/SiC/amorphous SiOC	~12.5	~9.1	−61	2.3 (4.2)	3.14	[50]
MWCNTs/SiC/amorphous SiOC	**6.0–13.0**	**0.7–4.3**	**−61.8**	**2.6 (4.2)**	**2.19**	**This work**

2.19 mm) at X-band. Compared with other polymer-derived ceramics (PDCs), the RL_{min} was higher and the thickness was thinner. The enhanced microwave-absorbing performance was due to interfacial polarization relaxation caused by the MWCNTs and SiC nanocrystals in the ceramic composites and the formed relatively complete conductive networks.

Acknowledgement

This work was supported by Shanghai Aerospace Science and Technology Innovation Fund (2017-121); Space Supporting Fund from China Aerospace Science and Industry Corporation (No. 2017-HT-XG); Natural Science Basic Research Plan in Shaanxi Province of China (No. 2018JM5001); Shenzhen Science and Technology Innovation Fund (No. JCYJ20170815155705061). We would like to thank the Analytical & Testing Center of Northwestern Polytechnical University for Transmission electron microscope (TEM) test.

References

[1] C. Wang, V. Murugadoss, J. Kong, Z. He, X. Mai, Q. Shao, Y. Chen, L. Guo, C. Liu, S. Angaiah, Z. Guo, Overview of carbon nanostructures and nanocomposites for electromagnetic wave shielding, Carbon 140 (2018) 696–733.
[2] B. Zhao, J. Deng, R. Zhang, L. Liang, B. Fan, Z. Bai, G. Shao, C.B. Park, Recent advances on the electromagnetic wave absorption properties of Ni based materials, Eng. Sci. 3 (2018) 5–40 www.doi.org/10.30919/es8d735.
[3] N. Wu, D. Xu, Z. Wang, F. Wang, J. Liu, W. Liu, Q. Shao, H. Liu, Q. Gao, Z. Guo, Achieving superior electromagnetic wave absorbers through the novel metal-organic frameworks derived magnetic porous carbon nanorods, Carbon 145 (2019) 433–444.
[4] C.J. Luo, T. Jiao, Y.S. Tang, J. Kong, Excellent electromagnetic wave absorption of iron-containing SiBCN ceramics at 1158 K high-temperature, Adv. Eng. Mater. (2018) 1701168.
[5] X.Y. Dai, Y.Z. Du, J. Yang, D. Wang, J.W. Gu, Y.F. Li, S. Wang, B.B. Xu, J. Kong, Recoverable and self-healing electromagnetic wave absorbing nanocomposites, Compos. Sci. Technol. 174 (2019) 27–32.
[6] Y.Z. Wang, X. Guo, Y.R. Feng, X. Lin, H.Y. Gong, Wave absorbing performance of polymer-derived SiCN(Fe) ceramics, Ceram. Int. 43 (17) (2017) 15551–15555.
[7] Y.Q. Guo, Z.Y. Lyu, X.T. Yang, Y.J. Lu, K.P. Ruan, Y.L. Wu, J. Kong, J.W. Gu, Enhanced thermal conductivities and decreased thermal resistances of functionalized boron nitride/poluimide composites, Compos. B Eng. 164 (2019) 732–739.
[8] D. Jiang, V. Murugadoss, Y. Wang, et al., Electromagnetic interference shielding polymers and nanocomposites – a review, Polym. Rev. (2019), https://doi.org/10.1080/15583724.2018.1546737.
[9] X.W. Yin, L. Kong, L.T. Zhang, L.F. Cheng, N. Travitzky, P. Greil, Electromagnetic properties of Si-C-N based ceramics and composites, Int. Mater. Rev. 59 (6) (2003) 326–355.
[10] P.C.P. Watts, W.K. Hsu, A. Barnes, B. Chambers, High permittivity from defective multiwalled carbon nanotubes in the X-band, Adv. Mater. 15 (7–8) (2010) 600–603.
[11] Q. Li, X.W. Yin, W.Y. Duan, B.L. Hao, L. Kong, X.M. Liu, Dielectric and microwave absorption properties of polymer derived SiCN ceramics annealed in N_2 atmosphere, J. Eur. Ceram. Soc. 34 (3) (2014) 589–598.
[12] Q. Li, X.W. Yin, W.Y. Duan, L. Kong, B.L. Hao, F. Ye, Electrical, dielectric and microwave-absorption properties of polymer derived SiC ceramics in X band, J. Alloy. Comp. 565 (28) (2013) 66–72.
[13] P. Colombo, G. Mera, R. Riedel, G.D. Soraru, Polymer-derived ceramics: 40 years of research and innovation in advanced ceramics, J. Am. Ceram. Soc. 93 (7) (2010) 1805–1837.
[14] C. Haluschka, C. Engel, R. Riedel, Silicon carbonitride ceramics derived from polysilazanes. Part 2: investigation of electrical properties, J. Eur. Ceram. Soc. 20 (9) (2000) 1365–1374.
[15] R. Raj, L.N. An, S. Shah, R. Riedel, C. Fasel, H.J. Kleebe, Oxidation kinetics of an amorphous silicon carbonitride ceramic, J. Am. Ceram. Soc. 84 (8) (2001) 1803–1810.
[16] S.H. Lee, E.R. Kupp, A.J. Stevenson, J.M. Anderson, G.L. Messing, X. Li, E.C. Dickey, Hot isostatic pressing of transparent Nd: YAG ceramics, J. Am. Ceram. Soc. 92 (7) (2009) 1456–1463.
[17] J.F. Li, K. Wang, B.P. Zhang, T. Ishii, L.M. Zhang, Ferroelectric and piezoelectric properties of fine-grained $Na_{0.5}K_{0.5}NbO_3$ lead-free piezoelectric ceramics prepared by spark plasma sintering, J. Am. Ceram. Soc. 89 (2) (2010) 706–709.
[18] M. Kumar, K.L. Yadav, Rapid liquid phase sintered Mn doped $BiFeO_3$ ceramics with enhanced polarization and weak magnetization, Appl. Phys. Lett. 91 (24) (2007) 6694.
[19] J. Meziere, M. Ucar, E. Blanquet, M. Pons, P. Ferret, L. Dicioccio, Modeling and simulation of SiC CVD in the horizontal hot-wall reactor concept, J. Cryst. Growth 267 (3) (2004) 436–451.
[20] W.Y. Duan, X.W. Yin, C.J. Luo, J. Kong, F. Ye, H.X. Pan, Microwave-absorption properties of SiOC ceramics derived from novel hyperbranched ferrocene-containing polysiloxane, J. Eur. Ceram. Soc. 37 (5) (2017) 2021–2030.
[21] C.J. Luo, W.Y. Duan, X.W. Yin, J. Kong, Microwave-absorbing polymer-derived ceramics from cobalt-coordinated poly(dimethylsilylene)diacetylenes, J. Phys. Chem. C 120 (33) (2016) 18721–18732.
[22] W.Y. Duan, X.W. Yin, Q. Li, X.M. Liu, L.F. Cheng, L.T. Zhang, Synthesis and microwave absorption properties of SiC nanowires reinforced SiOC ceramics, J. Eur. Ceram. Soc. 34 (2) (2014) 257–266.
[23] Y.J. Zhang, X.W. Yin, F. Ye, L. Kong, Effects of multi-walled carbon nanotubes on the crystallization behavior of PDCs-SiBCN and their improved dielectric and EM absorbing properties, J. Eur. Ceram. Soc. 34 (5) (2014) 1053–1061.
[24] F. Ye, L.T. Zhang, X.W. Yin, Y.J. Zhang, L. Kong, Y.S. Liu, L.F. Cheng, Dielectric and microwave-absorption properties of SiC nanoparticle/SiBCN composite ceramics, J. Eur. Ceram. Soc. 34 (2) (2014) 205–215.
[25] J.W. Gu, Q.Y. Zhang, J. Dang, C.J. Yin, S.J. Chen, Preparation and properties of polystyrene/SiCw/SiCp thermal conductivity composites, J. Appl. Polym. Sci. 124 (2012) 132–137.
[26] C.B. Liang, H. Qiu, Y.Y. Han, P. Song, H.B. Gu, L. Wang, J. Kong, J.W. Gu, D.P. Cao, Superior electromagnetic interference shielding 3D graphene nanoplatelets/reduced graphene oxide foam/epoxy nanocomposites with high thermal conductivity, J. Mater. Chem. C 7 (9) (2019) 2725–2733.
[27] X.Y. Yan, J.W. Gu, J. Guo, et al., Lowly loaded carbon nanotubes induced high electrical conductivity and giant magnetoresistance in ethylene/1-Octene copolymers, Polymer 103 (2016) 315–327.
[28] Y.M. Huangfu, C.B. Liang, Y.X. Han, H. Qiu, P. Song, L. Wang, J. Kong, J.W. Gu, Fabrication and investigation on the Fe_3O_4/thermally annealed graphene aerogel/epoxy electromagnetic interference shielding nanocomposites, Compos. Sci. Technol. 169 (2019) 70–75.
[29] L. Tang, J. Dang, M.K. He, J.Y. Li, J. Kong, Y.S. Tang, J.W. Gu, Preparation and properties of cyanate-based wave- transparent laminated composites reinforced by dopamine/POSS functionalized Keviar cloth, Compos. Sci. Technol. 169 (2019) 120–126.
[30] E. Ionescu, H.J. Kleebe, R. Riedel, Silicon-containing polymer-derived ceramic nanocomposites (PDC-NCs): synthesis approaches and properties, Chem. Soc. Rev. 43 (42) (2012) 5032–5052.
[31] E. Ionescu, C. Linck, C. Fasel, M. Müller, H.J. Kleebe, R. Riedel, Polymer-derived $SiOC/ZrO_2$ ceramic nanocomposites with excellent high-temperature stability, J. Am. Ceram. Soc. 93 (1) (2010) 241–250.
[32] E. Ionescu, B. Papendorf, H.J. Kleebe, F. Poli, K. Müller, R. Riedel, Polymer-derived silicon oxycarbide/hafnia ceramic nanocomposites. Part I: phase and microstructure evolution during the ceramization process, J. Am. Ceram. Soc. 93 (6) (2010) 1774–1782.
[33] K. Nakamoto, Y. Morimoto, A.E. Martell, Infrared spectra of metal chelate compounds. IV. Infraed spectra of addition compounds of metallic acetylacetonatesla, J. Am. Vhem. Soc. 83 (22) (1961) 4533–4536.
[34] Da Thornton, Infrared spectra of metal β-ketoenolates and related complexes, Coord. Chem. Rev. 104 (2) (1990) 173–249.
[35] D. Scarano, A. Zecchina, S. Bordiga, F. Geobaldo, G. Spoto, G. Petrini, G. Leofanti, M. Padovan, G. Tozzola, Fourier-transform infrared and Raman spectra of pure and Al-, B-, Ti- and Fe-substituted silicalites: stretching-mode region, J. Chem. Soc. Faraday. Trans. 89 (22) (1993) 4123–4130.
[36] M. Hojamberdiev, R.M. Prased, C. Fasel, R. Riedel, E. Ionescu, Single-source-precursor synthesis of soft magnetic Fe_3Si- and Fe_5Si_3-containing SiOC ceramic nanocomposites, J. Eur. Ceram. Soc. 33 (13–14) (2013) 2465–2472.
[37] J.S. Lee, Y.K. Byeun, S.H. Lee, S.C. Choi, In situ growth of SiC nanowires by carbothermal reduction using a mixture of low-purity SiO_2 and carbon, J. Alloy. Comp. 456 (1) (2008) 257–263.
[38] T. Vasilos, T. Ertürk, R. Ambati, SCS-6 SiC fiber reinforced fused silica composites,

Ceram. Eng. Sci. Proc. 14 (9) (2008) 955–962.
[39] H.P. Martin, R. Ecke, E. Muller, Synthesis of nanocrystalline silicon carbide powder by carbothermal reduction, J. Eur. Ceram. Soc. 18 (12) (1998) 1737–1742.
[40] X.Y. Wu, G.Q. Jin, X.Y. Guo, Effects of the amounts of Fe catalyst on stacking faults and morphologies of β-SiC, N. Carbon Mater. 20 (4) (2005) 324–328.
[41] M.K. Han, X.W. Yin, W.Y. Duan, S. Ren, L.T. Zhang, L.F. Cheng, Hierarchical graphene/SiC nanowire networks in polymer-derived ceramics with enhanced electromagnetic wave absorbing capability, J. Eur. Ceram. Soc. 36 (11) (2016) 2695–2703.
[42] A.C. Ferrari, J. Robertson, Interpretation of Raman spectra of disordered and amorphous carbon, Phys. Rev. B 61 (20) (2000) 14095–14107.
[43] J. Kong, M.J. Wang, J.H. Zou, L.N. An, Soluble and meltable hyperbranched polyborosilazanes toward high-temperature stable SiBCN ceramics, ACS Appl. Mater. Interfaces 7 (12) (2015) 6733–6744.
[44] W.F. Zhao, Y.S. Tang, J. Xi, J. Kong, Functionalized graphene sheets with poly(ionic liquid)s and high adsorption capacity of anionic dyes, Appl. Surf. Sci. 326 (2015) 276–284.
[45] L.L. Meng, X.F. Zhang, Y.S. Tang, K.H. Su, J. Kong, Hierarchically porous silicon-carbon-nitrogen hybrid materials towards highly efficient and selective adsorption of organic dyes, Sci. Rep. 5 (2015) 7910.
[46] A.C. Ferrari, J.C. Meyer, V. Scardaci, C. Casiraghi, M. Lazzeri, F. Mauri, S. Piscanec, D. Jiang, K.S. Novoselov, S. Roth, A.K. Geim, Raman spectrum of graphene and graphene layers, Phys. Rev. Lett. 97 (18) (2006) 187401.
[47] G.X. Zhu, Y.J. Liu, Z. Xu, T. Jiang, C. Zhang, X. Li, G. Qi, Flexible magnetic nanoparticles-reduced graphene oxide composite membranes formed by self-assembly in solution, ChemPhysChem 11 (11) (2010) 2432–2437.
[48] X.F. Zhang, Y.X. Li, R.G. Liu, Y. Rao, H.W. Rong, G.W. Qin, High-magnetization FeCo nanochains with ultrathin interfacial gaps for broadband electromagnetic wave absorption at gigahertz, ACS Appl. Mater. Interfaces 8 (5) (2016) 3494–3498.
[49] H. Chen, J. Kong, Hyperbranched polymers from A_2+B_3 strategy: recent advances in description and control of fine topology, Polym. Chem. 7 (22) (2016) 3643–3663.
[50] W.Y. Duan, X.W. Yin, F. Ye, Q. Li, M.K. Han, X.F. Liu, Y.Z. Cai, Synthesis and EMW absorbing properties of nano SiC modified PDC-SiOC, J. Mater. Chem. C 4 (25) (2016) 5962–5969.
[51] Z.J. Yu, H. Min, J.Y. Zhan, L. Yang, Preparation and dielectric properties of polymer-derived SiCTi ceramics, Ceram. Int. 39 (4) (2013) 3999–4007.